CHAPTER 13

Active Particles Propelled by Chemical Reactions

M.-J. HUANG, J. SCHOFIELD AND R. KAPRAL*

Chemical Physics Theory Group, Department of Chemistry, University of Toronto, Toronto, Ontario M5S 3H6, Canada
*Email: rkapral@chem.utoronto.ca

13.1 Introduction

Synthetic micro- and nano-scale motors that are able to move autonomously in solution using chemical energy supplied by the environment are interesting not only for their potential as agents in new devices but also because of the intriguing physics that arises in active systems operating out of equilibrium. These motors form a subset of a much broader class of natural and synthetic motors that use chemical reactions as a power source in order to perform a variety of functions.[1] Biological molecular machines use chemical energy to carry out active transport as well as a plethora of other biochemical functions in the cell. These molecular machines frequently utilize the chemical energy of adenosine triphosphate to produce conformational changes that allow them to execute directed motion. Because nanoscale machines experience strong thermal fluctuations from their environments they often operate while attached to biofilaments, perhaps in order to help mitigate some of the detrimental effects of thermal noise. Well-known examples of such machines include the numerous types of kinesin that walk on tubulin and carry out various transport tasks, and myosin motors that operate while attached to actin filaments.[2] On larger scales microorganisms

Theoretical and Computational Chemistry Series No. 14
Self-organized Motion: Physicochemical Design based on Nonlinear Dynamics
Edited by Satoshi Nakata, Véronique Pimienta, István Lagzi, Hiroyuki Kitahata and Nobuhiko J. Suematsu

Published by the Royal Society of Chemistry, www.rsc.org

also make use of chemically-powered conformational changes to swim in solution. For many such organisms the chemical energy is used to move flagella in a non-reciprocal cycle allowing them to swim in low Reynolds number environments where viscous effects dominate inertial effects.[3]

Synthetic motors have been constructed to mimic some of this behaviour. For example, molecular spiders made from linked nucleic acid catalysts are able to walk on a chemically-active patterned substrate that induces conformational changes to produce directed motion.[4] Artificial flagella made from linked colloidal magnetic particles driven by magnetic fields to execute non-reciprocal motions have been used to move red blood cells.[5] The synthetic motors we consider in this chapter have no moving parts and rely on phoretic mechanisms that arise from a coupling of the motor to a non-equilibrium environment to produce directed motion.[6] Bimetallic nanorod motors that are propelled by self-electrophoresis were some of the first such motors to be constructed.[7,8] Subsequently, a considerable amount of research, documented in reviews, has been carried out on a variety of motors with different shapes and propelled by different mechanisms.[6,9–12]

Here we focus on motors propelled by self-diffusiophoresis. In this mechanism catalytic chemical reactions taking place on a portion of the motor produce spatially inhomogeneous concentrations of reactants and products. Because these species interact with the motor through different intermolecular potentials, the concentration gradients give rise to a body force on the motor which, in turn, produces flow in a fluid environment.[13–15] Various kinds of motors that operate by this mechanism have been studied. These include, among others, spherical Janus motors comprising catalytic and non-catalytic hemispheres,[16–21] sphere-dimer motors made from linked catalytic and non-catalytic spheres,[22–24] nanowire motors,[25] polymer motors[26] and even oligomeric motors made from three linked spheres that walk on a filament[27] (see Figure 13.1). In order to sharpen the focus of our presentation further, most of our examples will deal with Janus motors but the general principles apply to other motor geometries, although analytical analysis is more difficult.

13.2 Propulsion by Self-diffusiophoresis

One of the simplest motor geometries is a spherical Janus motor with two surfaces that have different chemical activity. In experimental realizations, a Janus motor is made of a chemically-neutral spherical bead partially coated with catalytic material. For example, silica beads partially coated with platinum immersed in a solution of hydrogen peroxide fuel move autonomously.[17,28–30] Janus motors made by attaching enzymes to a portion of a spherical particle also move autonomously when placed in a solution containing substrate.[31] The motors in these two examples, and others like them,[32–34] derive their propulsion from the inhomogeneous distribution of reactants and products produced in the reaction on the asymmetric catalytic surface by the diffusiophoretic mechanism sketched above. One can see that

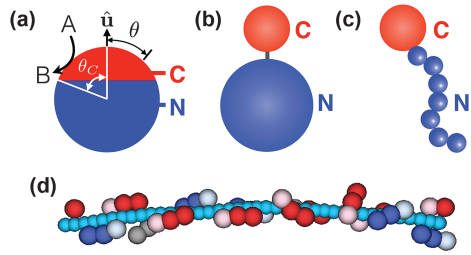

Figure 13.1 (a) A Janus motor has catalytic (*C*, red) and noncatalytic (*N*, blue) caps on the motor surface. The motor axis is defined by the unit vector, $\hat{\mathbf{u}}$, in the direction from the *N* to the *C* caps, and θ is the polar angle. Catalytic reactions occur when fuel *A* particles encounter the motor *C* surface and will be converted into product *B* particles. (b) and (c) are self-propelled sphere-dimer[22–24] and polymer nanomotors,[26] where the catalytic and noncatalytic beads are colored in red and blue, respectively. (d) shows three-bead oligomeric motors that walk on a filament (light blue beads). Motors are color coded by their orientation on the filament: a motor colored blue/red indicates that it is oriented so that the catalytic bead points to the right/left, where the catalytic beads in these motors are light blue/red. The gray beads belong to the motor that is detached from the filament.[27]

many different motor reactions can be used to produce propulsion. While the nature of the reaction mechanism on the motor surface and the interaction potentials of the fuel and product with the Janus motor will determine quantitative aspects of the motor dynamics, the basic propulsion principles can be understood by considering a simple irreversible $A \rightarrow B$ reaction on the catalytic face of the Janus motor and specific choices for the interaction potentials.

Because the motors of interest are small, with micron or nanometer sizes, thermal fluctuations of properties that characterize their dynamics are large relative to their average[20] and theoretical descriptions necessitate the use of a stochastic or molecular treatment of the dynamics. For large motors deterministic continuum models often can be used successfully to determine average motor velocities and steady state fluid flow and concentration fields. We shall use both coarse-grained microscopic simulation and continuum theory to study diffusiophoretic self-propulsion.

13.2.1 Microscopic Description

The construction of a microscopic model of active systems is conceptually straightforward. One simply specifies the form of the active particle and its interactions with the chemical species in the surrounding fluid, as well as the interactions among the fluid particles, and the fluxes of chemical species that maintain the system in a non-equilibrium state. Solution of the microscopic equations of motion for the entire system will then yield all

desired properties of the motor dynamics. Of course, this programme may be difficult to carry out because of the large number of particles, particularly of solvent type, in microscale or nanoscale systems. If the motor size is on the order of a few nanometers or less full molecular dynamics is required to describe the dynamics of the system because this is the regime where the molecular nature of the solvent makes itself felt most strongly.[35] On somewhat larger scales coarse-grained microscopic models where the interactions among the solvent molecules are accounted for through effective collisions may be used. In either case, provided the simplified dynamics preserves the basic conservation laws of mass, momentum and energy, the essential features of the dynamics will be preserved. This microscopic approach has the advantage that the diffusiophoretic mechanism emerges naturally from the dynamics, and in studies of the collective behaviour of many-motor systems all interactions through hydrodynamic flow fields and chemical concentration fields are accounted for.

Microscopic models of motors can be constructed in various ways. A collection of spherical catalytic and non-catalytic beads can be used as building blocks to make a roughly spherical Janus motor with catalytic and non-catalytic caps.[36] The fluid particles interact with the beads through soft intermolecular potentials that may depend on the bead and solvent species type. Chemical activity is also easily determined by the nature of the bead. This modeling scheme is not restricted to Janus motors and the sphere-dimer and oligomeric motors discussed above are made by linking beads with different catalytic properties. Microscopic simulations of motors propelled by thermophoretic mechanisms have also been carried out and have features in common with motors that operate by diffusiophoretic mechanisms.[37–39]

An even simpler Janus model is to suppose that the particle is a solid object that interacts with the fluid through hard bounce-back collisions.[21] While both the bead-aggregate and solid models have been used to study motor dynamics, below we shall present results for the solid model so it will be described in more detail. Specifically, the Janus motors are treated as solid spherical objects with a catalytic cap surface that is characterized by the angle θ_c defined from the north pole, indicated by the orientation vector $\hat{\mathbf{u}}$, to the interface between the catalytic C and non-catalytic N surfaces (see Figure 13.1(a)). Fluid particles at a distance r from the center of mass of Janus motor experience a hard sphere interaction potential:

$$W_\alpha(r) = \begin{cases} \infty, & r < R_\alpha \\ 0, & r \geq R_\alpha, \end{cases} \tag{13.1}$$

where R_α is the collision radius for a particle of type $\alpha = A, B$. The radius R of the Janus motor is chosen to be the larger of the two radii. Whenever a particle finds itself at a distance from the center of the motor that is less than the corresponding radius of its type, it will experience a modified bounce-back collision.[21] In each collision, a fluid particle exchanges both

linear and angular momentum with the Janus motor. The collision rules conserve the total energy as well as the total linear and angular momenta of the system.

Reactive events are easily described within this microscopic model and reactive collisions that correspond to different reaction mechanisms that satisfy the conservation laws can be constructed.[36] For example a simple irreversible $A \rightarrow B$ reaction catalysed by the motor can be implemented using reactive collisions that change the identity of fuel A to product B species with probability p_+ whenever an A particle encounters (*i.e.* comes within a distance R of) the catalytic surface with a polar angle $\theta < \theta_c$.

To extend the accessible time scales that can be probed in simulations, a coarse-grained model can be implemented in which the explicit interactions among fluid particles are accounted for through multiparticle collision dynamics, which is described in detail elsewhere.[40–43] The solvent multiparticle collisions are carried out at discrete collisions times and alter the particle velocities in a manner that is consistent with constants of motion so that mass, momentum and energy are conserved. On long distance and time scales the equations of continuum hydrodynamics can be derived from this microscopic dynamics.[40,41]

The final element in the microscopic model is the prescription for maintaining the system in a non-equilibrium state. This can be accomplished either by fixing the flux of reagents to pre-determined values at the boundaries of the system or by reactions in fluid phase that themselves take place under non-equilibrium conditions. In this latter case the reactive version of multiparticle collision dynamics may be used.[44] To establish a non-equilibrium steady state in a system where the reaction $A \rightarrow B$ occurs on the motor, it is sufficient to have reaction $B \rightarrow A$ in the fluid phase that destroy product and supply fuel.

13.2.2 Continuum Description

Usually propulsion by phoretic mechanisms is described by adopting a continuum perspective where the solute concentration and fluid velocity fields are governed by the diffusion and Stokes equations, respectively, subject to suitable boundary conditions for these fields. As noted earlier, self-propulsion is a non-equilibrium phenomenon and the system must be maintained in a non-equilibrium state for directed motion to occur. Here we suppose that a non-equilibrium steady state is established by including bulk-phase reactions $B \xrightarrow{k_2} A$,[†] while catalytic reactions, $C + A \rightarrow C + B$, on the motor surface generate species concentration gradient fields in the vicinity

[†]The rate constants in the bulk phase reaction are assumed to contain the constant concentrations of other reservoir species that maintain the system out of equilibrium and allow one to control the values of k_2. This overall reaction may itself be the result of a more complex mechanism.

of the motor. The steady-state concentration of B species, $c_B(r,\theta)$, can then be determined from the solution of the reaction-diffusion equations:

$$D\nabla^2 c_B(r,\theta) - k_2 c_B(r,\theta) = 0, \tag{13.2}$$

subject to the radiation boundary condition on the motor surface:

$$-k_D R\partial_r c_B(r,\theta)|_{r=R} = k_0 c_A(R,\theta)\Theta(\theta_C), \tag{13.3}$$

and $\lim_{r\to\infty} c_A = c_0$ far from the Janus motor. Here D is the common diffusion constant of fuel A and product B particles, k_0 is the intrinsic rate constant, $k_D = 4\pi DR$ is the Smoluchowski diffusion-controlled rate constant, $c_0 = c_A + c_B$ is the total constant bulk concentration of the reactive species, which we assume to hold locally, and $\Theta(\theta_C)$ is a characteristic function that is unity on the catalytic cap $(0 < \theta \le \theta_C)$ and zero on the non-catalytic cap $(\theta_C < \theta \le \pi)$. In view of the axial symmetry of the Janus motor and the fact that the concentration of B particles vanishes far from the motor, the steady-state solutions for the concentration field of B particles can be written as

$$c_B(r,\theta) = c_0 \sum_{\ell=0}^{\infty} a_\ell f_\ell(r) P_\ell(\mu), \tag{13.4}$$

where $P_\ell(\mu)$ is a Legendre polynomial with $\mu = \cos\theta$. After substitution of eqn (13.4) into eqn (13.2) and (13.3) the unknown functions $f_\ell(r)$ and coefficients a_ℓ can be determined. The function $f_\ell(r)$ is given by

$$f_\ell(r) = \frac{k_\ell(\kappa r)}{k_\ell(\kappa R)}, \tag{13.5}$$

where $k_\ell(\kappa r)$ are the modified spherical Bessel functions of the second kind and we have introduced the inverse screening length $\kappa = \sqrt{k_2/D}$. This function is defined such that $f_\ell(r = R) = 1$ and $f_\ell(r = \infty) = 0$. The coefficients can be found from the solution of a set of linear equations:

$$a_\ell = \sum_{m=0}^{\infty} (\mathbf{M}^{-1})_{\ell m} E_m, \tag{13.6}$$

where

$$M_{\ell m} = \frac{2Q_\ell}{2\ell+1}\delta_{\ell m} + \frac{k_0}{k_D}\int_{\mu_C}^{1} \mathrm{d}\mu P_\ell(\mu) P_m(\mu), \quad E_m = \frac{k_0}{k_D}\int_{\mu_C}^{1} d\mu P_m(\mu), \tag{13.7}$$

with $\mu_C = \cos\theta_C$ and $Q_\ell = \kappa R k_{\ell+1}(\kappa R)/k_\ell(\kappa R) - \ell$.

In a similar manner, the fluid velocity fields can be obtained by solving the Stokes equation, $\nabla p = \eta\nabla^2\mathbf{v}$, where p is the pressure field and $\mathbf{v}$ is the fluid velocity field, for an incompressible fluid $\nabla\cdot\mathbf{v} = 0$ subject to the boundary condition, $\mathbf{v}(R,\theta) = V_u\hat{\mathbf{u}} + \mathbf{v}^{(s)}$, where V_u is the propulsion speed of the motor, $\mathbf{v}^{(s)}$ is the slip velocity at the outer edge of the boundary layer, defined below,

and $\mathbf{v}(r=\infty)=0$ far from the motor. The components of the velocity field $\mathbf{v}=v_r\hat{\boldsymbol{r}}+v_\theta\hat{\boldsymbol{\theta}}$ are given by[45]

$$v_r(r,\mu)=V_u\left(\frac{R}{r}\right)^3 P_1(\mu)+\sum_{\ell=2}^{\infty}\ell(\ell+1)\left[\left(\frac{R}{r}\right)^{\ell+2}-\left(\frac{R}{r}\right)^{\ell}\right]\chi_\ell P_\ell(\mu), \tag{13.8}$$

$$v_\theta(r,\mu)=-\frac{V_u}{2}\left(\frac{R}{r}\right)^3 P_1^1(\mu)+\sum_{\ell=2}^{\infty}\left[(\ell-2)\left(\frac{R}{r}\right)^{\ell}-\ell\left(\frac{R}{r}\right)^{\ell+2}\right]\chi_\ell P_\ell^1(\mu). \tag{13.9}$$

where $\mathrm{P}_\ell^1(\mu)$ is the associated Legendre polynomial of order 1 and the coefficients χ_ℓ are related to the a_ℓ given in eqn (13.6) by $\chi_\ell=k_BT\Lambda c_0/(2\eta R)a_\ell$, where the explicit expression for the factor Λ is given in the next section.

These results for the continuum theory of the concentration and velocity fields can be compared with those obtained from microscopic simulations, and such a comparison will be presented below. Finally we note that an analogous set of calculations has been carried out for sphere-dimer motors using a bispherical coordinate system.[46]

13.2.3 Motor Propulsion Velocity

In the diffusiophoretic mechanism the body force on the motor due to the concentration gradients produced by the reaction at the catalytic cap on the motor gives rise to a velocity field in the surrounding fluid. The value of this velocity field at a distance $r=R$ at the outer edge of the boundary layer surrounding the particle where the interaction potentials of A and B particles with the Janus motor vanish is the slip velocity $\mathbf{v}^{(s)}(R,\theta)$. The axisymmetric slip velocity is given by

$$\mathbf{v}^{(s)}(R,\theta)=-\frac{k_BT}{\eta}\Lambda\nabla_\theta c_B(R,\theta), \tag{13.10}$$

where θ is the polar angle in a spherical polar coordinate system, ∇_θ is the gradient in the direction tangential to the motor surface, k_BT is the thermal energy, and η is the fluid viscosity. The effects of interactions with fluid particles of type $\alpha=A,B$ are accounted for by the factor, Λ, defined as

$$\Lambda=\int_0^\infty \mathrm{d}r\; r[\mathrm{e}^{-W_B(r)/k_BT}-\mathrm{e}^{-W_A(r)/k_BT}], \tag{13.11}$$

where $W_\alpha(r)$ is the interaction potential between an α-type fluid particle and the motor. For the hard potential given in eqn (13.1), $\Lambda=(R_A^2-R_B^2)/2$.

Once the slip velocity is known, the propulsion speed of the spherical Janus motor in the direction of its symmetry axis can be expressed as[13,14,47–49]

$$V_u=-\langle\hat{\mathbf{u}}\cdot\mathbf{v}^{(s)}\rangle_S, \tag{13.12}$$

where $\langle\cdots\rangle_S=(4\pi R^2)^{-1}\int_S \mathrm{d}S$ denotes the average over the motor surface at the outer edge of the boundary layer. Using eqn (13.4) for the concentration

field c_B of B particles in the equation of slip velocity, the propulsion speed of a hard sphere Janus motor is given by

$$V_u = \frac{2}{3}\frac{k_B T}{\eta}\frac{c_0}{R}\Lambda a_1 = \frac{1}{3}\frac{k_B T}{\eta}\frac{c_0}{R}(R_A^2 - R_B^2)a_1. \tag{13.13}$$

13.3 Dynamics of a Single Motor in Solution

It is interesting to compare the analytical results for the concentration and fluid flow fields obtained from the deterministic continuum model with microscopic simulations. For the sake of brevity we restrict our considerations to $\Lambda > 0$ so that the motor self-propulsion is in the $+\hat{\mathbf{u}}$ direction. The structures of these fields depend sensitively on the size of the catalytic cap, and the changes in the fields with cap size will be described.

Figure 13.2 compares the continuum theory and microscopic simulation[‡] results for the steady-state product concentration field, $c_B(\mathbf{r})$, for three different catalytic cap sizes corresponding to $\theta_C = 30^\circ$, 90° and 150°. As anticipated, c_B attains its maximum value on the catalytic surface and decreases in both the radial and tangential directions. The location of the maximum in the tangential concentration gradient field, $\nabla_\theta c_B$, on the motor surface varies with the size of the catalytic cap. This induces changes in the slip velocity which, in turn, significantly changes the flow fields in the surrounding fluid. We see from the figure that the concentration fields obtained from the solution of the reaction-diffusion equation agree quite well with the microscopic simulation results, although there are noticeable differences.

The microscopic simulation results for the variations of the near-field fluid velocity in the vicinity of the Janus motor as a function of θ_C are shown in Figure 13.3. For a Janus motor with a small catalytic cap ($\theta_C = 30^\circ$), the interface between the catalytic C and non-catalytic N portions of the Janus motor lies near the head of the sphere, termed the north pole, with a direction given by the polar axis vector $\hat{\mathbf{u}}$. Because $\nabla_\theta c_B$ is large at the interface, a strong velocity field is induced in this region that moves fluid particles from the front of the motor to the lateral directions; the weaker solvent flow field at the south pole is also incoming to the motor surface. The flows are in the opposite directions when the cap size is large ($\theta_C = 150^\circ$); the interface is close to the south pole of the motor producing a flow field that takes fluid particles from the lateral directions to the non-catalytic surface, whereas an outgoing flow at the north pole is induced by motor motion. For the Janus motor with $\theta_C = 90^\circ$, the flow fields in the front and rear of the Janus motor are largely determined by the motion of the motor-producing flows away from the motor in the region directly ahead of the motor whereas a more

[‡]The interaction radii for the hard sphere interactions are $R_A = 2.5$ and $R_B = 2.45$ and the systems are maintained in a non-equilibrium steady state by using an irreversible bulk reaction $B \to A$ with rate constant $k_2 = 0.001$. Simulation details can be found in ref. 21 and 50.

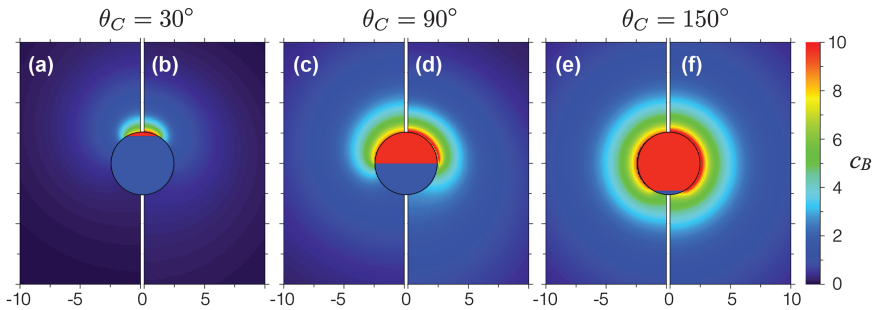

Figure 13.2 Product concentration field, $c_B(r,\theta)$, for Janus motors with catalytic cap size of $\theta_C = 30°$ (left), 90° (middle) and 150° (right). Panels (a), (c) and (e) are obtained from the expressions in eqn (13.8) and (13.9), whereas (b), (d) and (f) are the results obtained from simulations using the hard sphere model.[50] The catalytic and the noncatalytic hemispheres are labeled in red and blue, respectively.

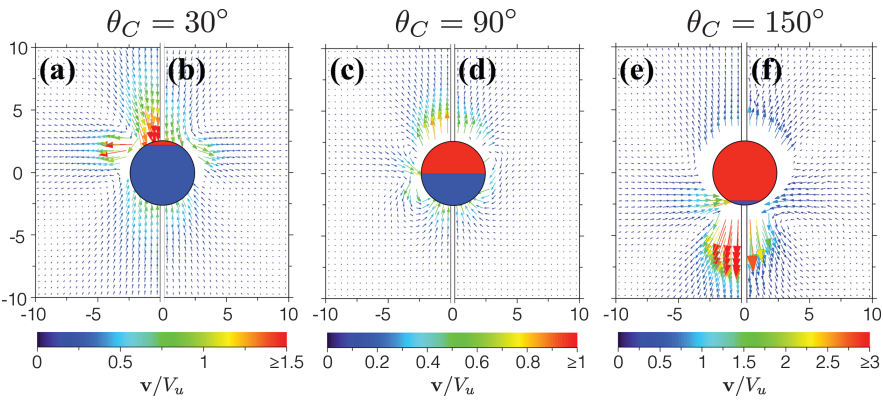

Figure 13.3 The induced flow field ($\mathbf{v}$) normalized by the propulsion speed (V_u) for three different sizes of the catalytic surface: $\theta_C = 30°$ (left), 90° (middle) and 150° (right). Panels (a), (c) and (e) are obtained from the expressions in eqn (13.8) and (13.9), whereas (b), (d) and (f) are the results obtained from simulations using the hard sphere model.[50] The catalytic and the noncatalytic hemispheres are labeled in red and blue, respectively.

complicated fluid circulation pattern is observed at the lateral direction of the motor.

Examination of the figure shows that while the continuum theory captures the gross structural features of these flow fields there are significant quantitative differences between the continuum theory flow fields and those observed in the microscopic simulations. These deviations are probably due to the microscopic details of the dynamics within the boundary layer that are

not captured by the boundary conditions utilized to solve the continuum equations for the flow and concentration fields.

A similar comparison has been carried out for sphere dimer motors.[46] For sphere dimers, where the catalytic activity is confined to the entire surface of the catalytic sphere, the analogue of the variable cap size in a Janus motor is a difference in the size of the catalytic sphere in the dimer relative to that of the non-catalytic sphere.

13.4 Dynamics of Systems with Many Motors

When the system contains many active particles, interactions among them from a number of different sources can give rise to collective behaviour that is different from suspensions of inactive particles.[6,9,19,27,30,32–34,48,51–70] Even in the absence of any attractive interactions active particles can undergo motility-induced phase separation where the active particles segregate into domains of high and low density.[55] Simple active Brownian models can capture the dynamics of this process. The Langevin equations of motion of the spherical active particles are given by

$$\frac{\mathrm{d}\mathbf{R}_i}{\mathrm{d}t} = \mu(\mathbf{F}_i^p + \mathbf{F}_i) + \mathbf{f}_i^t \tag{13.14}$$

$$\frac{\mathrm{d}\hat{\mathbf{u}}}{\mathrm{d}t} = \mathbf{f}_i^r \times \hat{\mathbf{u}}_i, \tag{13.15}$$

where $\mathbf{R}_i$ and $\hat{\mathbf{u}}_i$ are the position and orientation of active particle i, and $\mu = 1/\zeta$ is the mobility for friction coefficient ζ. In the active Brownian model, the self-propulsion force is a constant $\mathbf{F}_i^p = \zeta V_u \hat{\mathbf{u}}_i$, and the short-range repulsive force between particles is given by $\mathbf{F}_i = \sum_{j \neq i} \mathbf{F}_{ij}$, where $\mathbf{F}_{ij} = -\mathbf{F}_{ji}$ is the force between motors i and j. The system is subject to thermal fluctuations described by $\mathbf{f}_i^t$ and $\mathbf{f}_i^r$, which satisfy fluctuation-dissipation relations, $\langle \mathbf{f}_i^t(t)\mathbf{f}_j^t(t')\rangle = 2D_0\delta_{ij}\mathbf{1}\delta(t-t')$ and $\langle \mathbf{f}_i^t(t)\mathbf{f}_j^t(t')\rangle = 2D_0^{\mathrm{R}}\delta_{ij}\mathbf{1}\delta(t-t')$, where $D_0 = k_BT/\zeta$ and $\mathrm{D}_0^{\mathrm{R}} = (2\tau_R)^{-1}$ are the translational and rotational diffusion coefficients with the rotational relaxation time τ_R.

The clustering mechanism can be understood in terms of fluxes at the interface between the low and dense phases. A flux that brings particles into a dense region in the system is proportional to the motor propulsion speed V_u, whereas the outgoing flux is determined by the timescale τ_R for rotational diffusion to alter the direction of an active particle moving toward the dense phase. Clustering occurs when the incoming flux is greater than the outgoing flux, *i.e.* a larger motor speed and slower rotational diffusion gives rise to a greater tendency to aggregate. The relative importance of these two effects is characterized by the Péclet number $\mathrm{Pe} = |V_u|\ \tau_R/R$, where R is the particle radius. Another factor that affects phase behaviour is the concentration of motors typically expressed as an area or volume fraction ϕ.

Numerical and analytical studies of active Brownian systems have found different phases that can be characterized in a phase diagram in the Pe-ϕ plane.[54–56,58,71–74] Neither hydrodynamic nor concentration-mediated interactions that are important for chemically-powered motors are taken into account in the active Brownian model.

In the overdamped limit where inertia is unimportant a force applied at a given point in the fluid immediately gives rise to a velocity field at distant points in the fluid leading to fluid-mediated hydrodynamic forces that couple the motion of solutes that are not interacting directly. In systems of self-propelled motors the entire system is force-free, and this fact imposes conditions on the forms that these hydrodynamic interactions take. The induced flow from motor j modifies the velocity of motor i and adds an additional term to eqn (13.14) of the form $\sum_{j \neq i} \mathbf{v}_j(\mathbf{R}_i; \mathbf{R}_j, \hat{\mathbf{u}}_j)$ where $\mathbf{v}_j(\mathbf{R}_i; \mathbf{R}_j, \hat{\mathbf{u}}_j)$ is the velocity field at the position of motor i produced by motor j at position $\mathbf{R}_j$ with orientation $\hat{\mathbf{u}}_j$, and a similar treatment can be applied to the angular velocity.[75–77] Such hydrodynamic couplings among active swimmers has been studied.[3,61,78–83] 'Puller' swimmers induce an incoming fluid flow along the swimming axis bringing other swimmers together along this direction, and outgoing flows in the lateral directions give rise to an effective repulsion in the perpendicular directions. For 'pusher' swimmers, the hydrodynamic flows are reversed (see Figure 13.4).

Stochastic models that neglect hydrodynamic interactions but include concentration-mediated interactions can be described by the dynamical equations,

$$\frac{\mathrm{d}\mathbf{R}_t}{\mathrm{d}t} = -b_1 \nabla c_B(\mathbf{R}_i) + \mu(\mathbf{F}_i^p + \mathbf{F}_i) + \mathbf{f}_i^t \tag{13.16}$$

$$\frac{\mathrm{d}\hat{\mathbf{u}}_i}{\mathrm{d}t} = -b_2(1 - \hat{\mathbf{u}}_i\hat{\mathbf{u}}_i) \cdot \nabla c_B(\mathbf{R}_i) + \mathbf{f}_i^r \times \hat{\mathbf{u}}_i, \tag{13.17}$$

where $c_B(\mathbf{R}_i)$ is the local concentration of product particles around motor i produced by other active particles, and the magnitudes of the response of a

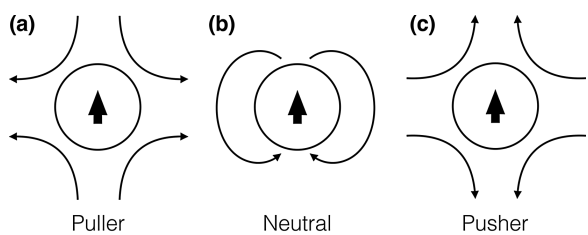

Figure 13.4 The sketch of fluid flows induced by (a) a puller swimmer, (b) a neutral swimmer and (c) a pusher swimmer, where the stream lines indicate flow fields and the arrow at the center of a swimmer shows swimming direction.

motor to the concentration field gradient are given by the parameters $b_{1,2}$ which are proportional to the interaction factor Λ. The parameter b_1 determines the effective interactions between active particles; a concentration-mediated interaction is attractive if $b_1 > 0$ (chemotactic attraction) and is repulsive if $b_1 < 0$ (chemotactic repulsion). The parameter b_2 determines the orientational ordering of motors along ($b_2 > 0$) and against ($b_2 < 0$) the gradient in the concentration of product particles. Numerical simulations of such systems have been performed and several different phases have been observed, including gas-like phases, dynamic cluster states and other time-dependent and collapsed cluster states.[67,68,84,85]

13.4.1 Microscopic Description of Active Particle Collective Motion

Unlike continuum theories that rely on various approximations to describe the collective behaviour of active systems, microscopic models naturally account for direct intermolecular interactions, many-body concentration gradients, fluid flows and thermal fluctuations. We now describe some of the results of microscopic simulations of the collective motion of diffusiophoretic motors. In particular, we shall discuss the interplay between chemotactic and hydrodynamic interactions and how these two effects influence motor collective dynamics.

Microscopic descriptions of the collective dynamics of motors propelled by diffusiophoretic mechanisms have been carried out for sphere-dimer motors,[65,70] as well as three-bead oligomeric motors moving on filaments in solution.[27] The non-spherical shapes of sphere-dimer motors, along with coupling interactions arising through chemical and hydrodynamic effects give rise to cluster states whose structural and dynamic properties depend on all of these factors. The confinement of oligomeric motors to filaments leads to distinctive correlations among the motors that depend strongly on chemical gradients. The collective behaviour of dimer motors propelled by thermophoresis has been studied and flattened swarms of motors have been shown to arise from a combination of phoretic repulsion and hydrodynamic lateral attraction.[86] We now describe some aspects of the collective behaviour of hard spherical Janus motors that interact with one another through repulsive Lennard–Jones interactions $V_{LJ}(r) = 4\epsilon[(\sigma/r)^{12} - (\sigma/r)^6 + 1/4]\Theta(r_c - r)$, where $\Theta(r_c - r)$ is a Heaviside function and the cut-off distance $r_c = 2^{1/6}\sigma$. We take $\epsilon = 1$ and $\sigma = 6$.

The propulsion arising from the diffusiophoretic mechanism is accompanied by concentration gradient and slip velocity fields at the motor surface that determine the coupling of the motor to the surrounding fluid. As already discussed in Section 13.3, these two fields change significantly with the size of the catalytic cap on the spherical Janus motor. Depending on the characteristics of the induced flow fields, chemotactic and hydrodynamic interactions can work either cooperatively or against one another to enhance or suppress dynamical clustering.[50] In the simulations described below, while

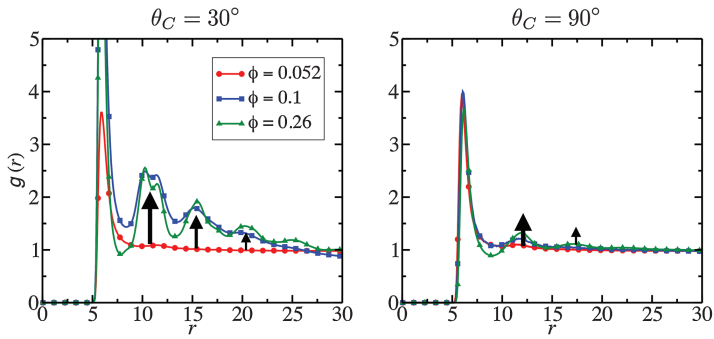

Figure 13.5 Radial distribution functions, $g(r)$, for the systems of Janus motors with various sizes of catalytic cap with $\theta_C = 30^\circ$ and 90° at volume fractions $\phi = 0.052$ (red circles), 0.1 (blue squares) and 0.26 (green triangles). The black arrows indicate the changes of $g(r)$ as ϕ increases.

the chemotactic interaction is chosen to be always attractive,[§] hydrodynamic interactions can be attractive or repulsive depending on the characteristics of the induced flow fields and motor spatial configurations. Going from small to large cap sizes, the Janus motor may be classified in terms of the near-field flows (see Figure 13.3) as a puller swimmer for small caps ($\theta_C = 30^\circ$), a neutral swimmer for intermediate-size caps ($\theta_C = 90^\circ$) and a pusher swimmer for large size caps ($\theta_C = 150^\circ$). Depending on the size of the catalytic cap the hydrodynamic interactions may enhance or reduce chemotactic attraction for small ($\theta_C = 30^\circ$) or large cap sizes ($\theta_C = 90^\circ$), respectively.

The clustering behaviour that arises from these interactions can be described quantitatively by the radial distribution function, $g(r)$, for different types of Janus motors in systems with motor volume fractions $\phi = 0.052$, 0.1 and 0.26,[¶] as shown in Figure 13.5. The enhanced clustering for Janus motors with small catalytic caps is evident from the comparison of the radial distribution functions of motors with $\theta_C = 30^\circ$ and 90°. Going from small to large volume fractions, it is clear to see that while only weak clustering is seen in the system of Janus motors with $\theta_C = 90^\circ$, strongly enhanced clustering is observed for Janus motors with $\theta_C = 30^\circ$ at the positions of the nearest ($r \simeq \sigma$) and next-nearest ($r \simeq 2\sigma$) neighbours, where $\sigma = 6$ is the distance in the repulsive Lennard–Jones potential.

Additional information concerning the effects of hydrodynamic flows on the Janus motor dynamics can be obtained from an examination of the motor velocity fields, as shown in Figure 13.6. Focusing on a specific motor,

[§]Simulations were performed using the hard sphere model for the Janus motors. The interaction radii are chosen to be $R_A = 2.5$ and $R_B = 2.35$ so that $\Lambda = (R_A^2 - R_B^2)/2 > 0$, indicating an effective attraction toward high product concentration regions. Simulation details can be found in ref. 21 and 50.

[¶]The volume fraction of Janus motors is $\phi = (NV_c)/V$, where $V_c = \frac{1}{6}\pi\sigma^3$ is the effective volume of a Janus motor, $V = 60^3$ is the system volume, and $N = 100$, 200 and 500 is the total number of Janus motors in the system.

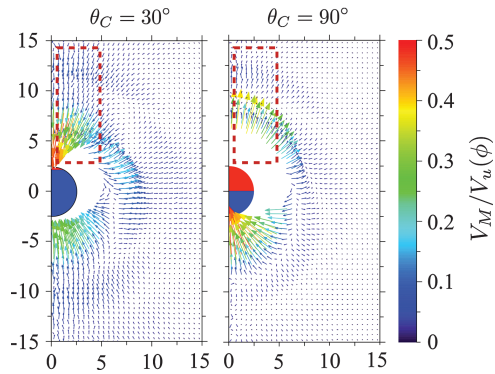

Figure 13.6 Motor velocity fields, $\mathbf{V}_M(r, \theta)$, at volume fraction $\phi = 0.1$ for catalytic cap sizes $\theta_C = 30^\circ$ and 90° normalized by the average motor propulsion speed, $V_u(\phi) = 0.0078$ and 0.014, respectively. The region in front of the motor, where chemotactic interactions are the strongest, is highlighted by red dashed rectangle.

one can see that while there are incoming motor flows toward the rear of the motor for both types of Janus motor, the dynamical behaviour of neighbouring motors in front of the motor differs substantially when the cap size changes. The red-dashed rectangles highlight the nearest and the next nearest regions in front of the motor. One can see that the average motor flow velocity points inward toward the surface of the motor for small cap sizes, while for large cap sizes the motor flow velocities are outgoing from the motor surface.

13.4.2 Microscopic Dynamics with Chemical Coupling Removed

In order to gauge the relative importance of chemotactic and hydrodynamic interactions one must be able to selectively turn off these interactions in simulations while not disturbing the diffusiophoretic mechanism of self-propulsion for single motors that involves both local concentration gradients and coupling to fluid flow. This can be achieved by considering a collection of Janus motors in which each motor i, instead of common product particles, produces a distinct product B_i that interacts with motor i as a product particle but as a non-reactive A particle with all other motors j. In this way only the self-generated concentration gradient of B_i is responsible for the propulsion of that motor. In this model the concentration-mediated chemotactic attraction is turned off while hydrodynamic interactions between Janus motors resulting from self-propulsion remain.[27]

As a consequence of the absence of chemotactic interactions, starting from an initial cluster configuration displayed in Figure 13.7, the cluster gradually breaks apart and the system reaches a steady state in which the Janus motors are homogeneously distributed beyond the first solvation

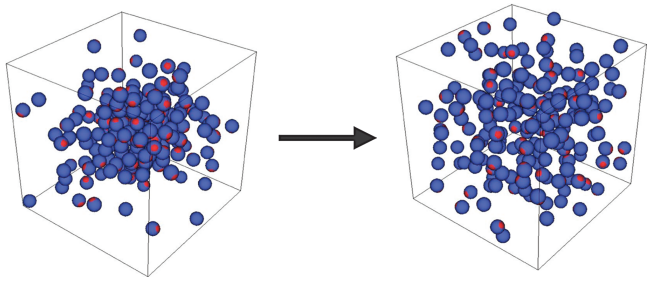

Figure 13.7 Starting from a cluster configuration of Janus motors with small cap sizes (left figure), when chemotactic interactions are turned off the cluster breaks apart to form a homogeneous distribution of Janus motors (right figure).

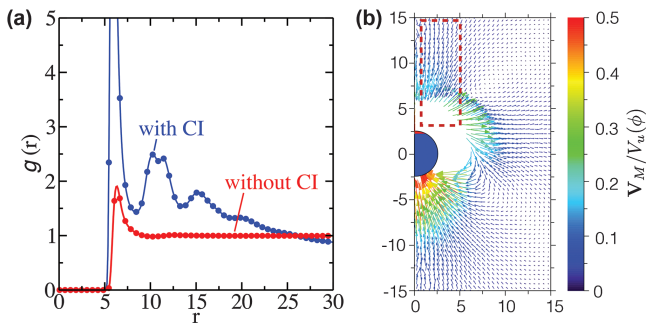

Figure 13.8 The radial distribution function, $g(r)$, and motor velocity fields, $\mathbf{V}_M$, for the Janus motor with catalytic cap size $\theta_C = 30^\circ$ in the absence of chemotactic interactions. In the left panel, $g(r)$ for the system with chemotactic interactions is plotted for comparison.

shell. The disappearance of clustering in the absence of concentration-mediated interactions is reflected in the lack of structure in the radial distribution function, and in the changes in structure of the motor velocity fields (see Figure 13.8). The changes observed in the radial distribution function indicate that turning off chemotactic interactions has a significant impact on the motor velocity fields at short distances but a weaker influence at long distances. These results show that long-ranged interactions are mediated by hydrodynamic interactions, which bring Janus motors toward each other, while the short-range interactions are primarily due to chemotactic effects.[50]

13.5 Dynamics of Motors in Crowded Media

While the motion of a chemically-powered motor in a simple fluid environment has been studied often, this is not the case for more complex solutions;

for example, those containing suspended colloidal particles. Here we survey some of the new features that arise for motor motion in such environments.

First, we consider a system comprising a single Janus motor with catalytic and non-catalytic hemispheres ($\theta_C = 90^\circ$) immersed in a fluid containing N_p passive spherical particles. The Janus motor and passive particles are taken to be hard solid objects that interact with each other through the repulsive Lennard–Jones potentials introduced earlier in the discussion of Janus motor collective behaviour. We again take $\epsilon = 1$ and $\sigma = 6$ so that the effective volume of a motor or passive particle is $V_c = \frac{1}{6}\pi\sigma^3$. For a system with volume $V = 60^3$ containing a single motor and $N_p = 599$ passive particles in the fluid medium, the volume fraction of suspended particles is $\phi = (NV_c)/V \simeq 0.3$, where $N = N_p + 1$. Further simulation details can be found in ref. 87.

The influence of motor activity on the properties of inert solutes can be seen by comparing the structures of the radial distributions of passive particles and fuel particles in the vicinity of chemically-active ($\Lambda > 0$ with $R_A = 2.5$ and $R_B = 24$) and chemically-inactive ($\Lambda = 0$ with $R_A = R_B = 2.5$) Janus motors. The radial distribution function of passive particles around the active and inactive Janus motor is given by

$$g(r) = \frac{V}{4\pi r^2 N_p} \left\langle \sum_{i=1}^{N_p} \delta(r_{Ji} - r) \right\rangle, \tag{13.18}$$

where r_{Ji} is the distance between the centre of the Janus motor and passive particle i, and $\langle \cdots \rangle$ denotes the steady-state time and ensemble average over trajectories. Figure 13.9(a) compares the radial distribution $g(r)$ around two

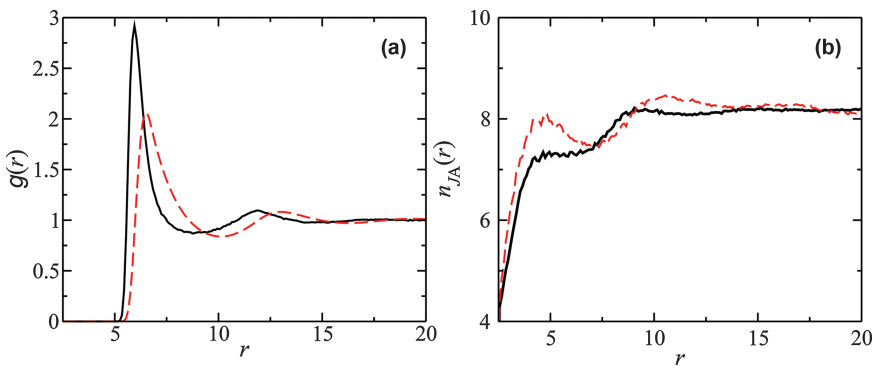

Figure 13.9 (a) The radial distribution function, $g(r)$, between the Janus motor and the surrounding obstacles and (b) the average density of the fuel A particles as a function of distance from the center of the motor. The black solid curves in (a) and (b) are for active Janus motor (with propulsion), whereas the red dashed curves are for passive Janus motor (without propulsion).

types of Janus motor. One can see that the positions of the peaks for active Janus motor lie at shorter separations, indicating a more packed structural ordering of the surrounding passive particles induced by motor self-propulsion.

As a result of this packing of the passive particles around the Janus motor, the density of chemical species varies in the radial direction from the Janus motor. The steady-state density of fuel particles around the Janus motor is given by:

$$n_A(r) = \frac{1}{4\pi r^2}\left\langle \sum_{i=1}^{N_A(t)} \delta(r_{Ji} - r) \right\rangle, \tag{13.19}$$

where $N_A(t)$ is the instantaneous number of fuel particles in the system, and r_{Ji} is the separation between the Janus motor position and fuel particle i. As can be seen in Figure 13.9(b), fuel particles are depleted at the mean positions of passive particles at $r \approx 6$. As expected, the spherically-averaged fuel density in the vicinity of an inactive Janus motor is higher than that for an active particle because no chemical reaction occurs on its surface.

Second, we reverse the situation and consider systems with a single passive particle in an active medium of N_J Janus motors. The Janus motors and passive particle are the same as above but we consider both forward-moving ($\Lambda > 0$) and backward-moving ($\Lambda < 0$) motors. As discussed above, the collective behaviour of forward-moving and backward-moving Janus motors is different; for example transient clusters arising from concentration-mediated interactions are observed in a collection of forward-moving motors, while in a system of backward-moving motors no significant directional and orientational ordering exists.[21] Consequently, one may expect that a passive particle will behave differently when immersed in these two types of active media.

The volume fraction dependence of the diffusion coefficient of the passive particle determined from the long-time behaviour of the mean square displacement is given in Table 13.1. This table compares the diffusion coefficients D^F and D^B of the passive particle in media with active with forward-moving and backward-moving Janus motors, respectively, with D' in a medium with inactive Janus motors. While D' decreases as ϕ increases in

Table 13.1 Dependence of the passive particle diffusion coefficient on the volume fraction in a medium with inactive Janus motors (D') and media with active with forward-moving (D^F) and backward-moving (D^B) Janus motors.

ϕ	0.05	0.1	0.16	0.21	0.26	0.3
$D'(\phi)$	0.0030	0.0029	0.0026	0.0024	0.0021	0.0018
$D^F(\phi)$	0.0045	0.0054	0.0064	0.0056	0.0071	0.0068
$D^B(\phi)$	0.0040	0.0052	0.0052	0.0050	0.0056	0.0052

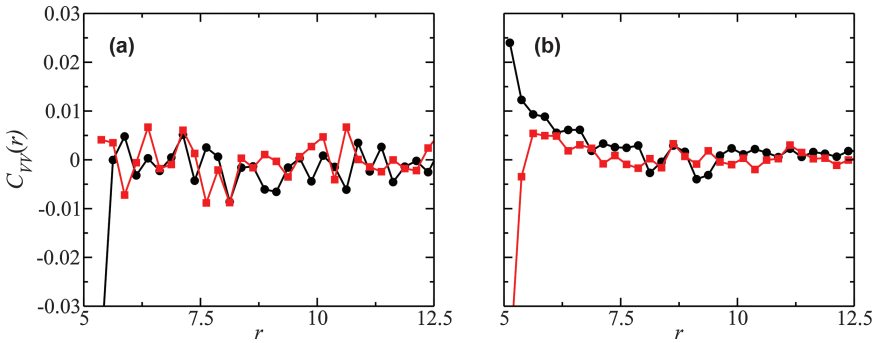

Figure 13.10 Velocity correlation, $C_{VV}(r)$, between the single passive tracer particle and the surrounding forward-moving (black circles) or backward-moving (red squares) Janus motors with volume fraction (a) $\phi = 0.05$ and (b) $\phi = 0.3$.

the inactive Janus medium, a strong enhancement of the diffusion coefficient at high volume fractions is found in media with forward-moving Janus motors, and a less significant enhancement is found in media with backward-moving motors.

The origin of the activity dependence of the passive particle diffusion coefficient can be understood by considering the correlation between the velocity of the passive particle and active motors, as expressed in the correlation function $C_{VV}(r)$ defined as

$$C_{VV}(r) = \frac{1}{n(r)} \left\langle \sum_{i=1}^{N_J} (\hat{\mathbf{v}}_T \cdot \hat{\mathbf{v}}_i) \delta(r_{Ti} - r) \right\rangle, \tag{13.20}$$

where $\hat{\mathbf{v}}_T = \mathbf{v}_T/|\mathbf{v}_T|$ and $\hat{\mathbf{v}}_i = \mathbf{v}_i/|\mathbf{v}_i|$ are the unit vectors determined by the velocities of the passive particle and active particle i, respectively, and $n(r) = \left\langle \sum_{i=1}^{N_J} \delta(r_{Ti} - r) \right\rangle$ is the average number of passive particle-motor pairs with separation $r_{Ti} = |\mathbf{r}_T - \mathbf{r}_i|$ at r. Figure 13.10 shows this correlation function in (a) dilute and (b) dense media with forward-moving (black circles) and backward-moving (red squares) motors. While no significant correlation at any distance r is found in dilute systems, for forward-moving motors positive correlations in the passive particle and motor velocities are observed at both short ($r \simeq 5$) and intermediate ($5 < r < 7.5$) separations. In contrast, $C_{VV}(r)$ decreases at small separations for the system with backward-moving motors. Recall that transient clusters were observed for forward-moving Janus motors, whereas no significant cluster formation was seen backward-moving motors.[21] The positive velocity correlation seen in Figure 13.10(b) for forward-moving Janus motors suggests that the passive particle is encapsulated by and moves collectively with surrounding Janus motors in dense

active media. By this entrainment mechanism, the mobility of a passive particle in a crowded environment can be significantly enhanced.

13.6 Conclusion

Synthetic self-propelled motors come in all shapes and sizes and can be tailored to perform specific tasks. These features have stimulated the increasing research effort that is devoted to their construction and the exploration of their potential applications, in particular at the nanoscale. Theory and simulation play an important role in this research because they can be used to elucidate the mechanisms by which these motors operate and provide predictions for their properties. This field of research also presents challenges for theory, especially for very small motors for which continuum theory may not be applicable.

Motors that are powered by chemical energy and operate by phoretic mechanisms pose special challenges. The collective behaviour that such systems display is governed by an interplay of direct intermolecular forces, hydrodynamic interactions and interactions determined by chemical gradients that operate on both short and long distance and time scales. It is difficult to incorporate all of these features into simple many-body phenomenological models. Microscopic simulation methods that treat the multi-component fluid in which the motors move on a particle-based level can account for all of these interactions. The results presented in this chapter should serve to show how coarse-grained microscopic models can be constructed and used to explore various aspects of the dynamics of motors propelled by self-diffusiophoresis. Through a combination of experiment, theory and simulation one can explore the new phenomena that arise in these active particle systems.

Acknowledgements

This research was supported in part by grants from the Natural Sciences and Engineering Research Council of Canada.

References

1. R. A. L. Jones, *Soft Machines: Nanotechnology and Life*, Oxford University Press, Oxford, 2004.
2. B. Alberts, D. Bray, J. Lewis, M. Raff, K. Roberts, and J. D. Watson, *Molecular Biology of the Cell*, Garland Science, 3rd edn, 2002.
3. E. Lauga and T. R. Powers, The hydrodynamics of swimming microorganisms, *Rep. Prog. Phys.*, 2009, **72**, 096601.
4. R. Pei, S. K. Taylor, D. Stefanovic, S. Rudchenko, T. E. Mitchell and M. N. Stojanovic, Behavior of polycatalytic assemblies in a substrate-displaying matrix, *J. Am. Chem. Soc.*, 2006, **128**, 12693–12699.
5. R. Dreyfus, J. Baudry, M. L. Ropar, M. Fermigier, H. A. Stone and J. Bibetter, Microscopic artificial swimmers, *Nature*, 2005, **437**, 862.

6. R. Kapral, Perspective: Nanomotors without moving parts that propel themselves in solution, *J. Chem. Phys.*, 2013, **138**, 020901.
7. W. F. Paxton, K. C. Kistler, C. C. Olmeda, A. Sen, S. K. St. Angelo, Y. Cao, T. E. Mallouk, P. E. Lammert and V. H. Crespi, Catalytic nanomotors: Autonomous movement of striped nanorods, *J. Am. Chem. Soc.*, 2004, **126**, 13424.
8. S. Fournier-Bidoz, A. C. Arsenault, I. Manners and G. A. Ozin, Synthetic self-propelled nanorotors, *Chem. Commun.*, 2005, 441.
9. J. Wang. *Nanomachines: Fundamentals and Applications*. Wiley-VCH, Weinheim, 2013.
10. S. Sánchez, L. Soler and J. Katuri, Chemically powered micro- and nanomotors, *Angew. Chem., Int. Ed.*, 2014, **53**, 2–33.
11. Y. Tu, L. K. E. A. Abdelmohsen, F. Peng and D. A. Wilson, Micro- and nano-motors for biomedical applications, *J. Mater. Chem. B*, 2014, **2**, 2395.
12. K. Dey, F. Wong, A. Altemose and A. Sen, Catalytic motorsquo vadimus?, *Curr. Opin. Colloid Interface Sci.*, 2016, **21**, 4–13.
13. J. L. Anderson, Colloid transport by interfacial forces, *Phys. Fluids*, 1983, **26**, 2871.
14. J. L. Anderson, Colloid transport by interfacial forces, *Ann. Rev. Fluid Mech.*, 1989, **21**, 61–99.
15. F. Jülicher and J. Prost, Generic theory of colloidal transport, *Eur. Phys. J.*, 2009, **29**, 27–36.
16. R. Golestanian, T. B. Liverpool and A. Ajdari, Designing phoretic micro- and nano-swimmers, *New J. Phys.*, 2007, **9**, 126.
17. H. Ke, S. Ye, R. L. Carroll and K. Showalter, Motion analysis of self-propelled pt-silica particles in hydrogen peroxide solutions, *J. Phys. Chem. A*, 2010, **114**, 5462.
18. B. Sabass and U. Seifert, Dynamics and efficiency of a self-propelled, diffusiophoretic swimmer, *J. Chem. Phys.*, 2012, **136**, 064508.
19. I. Theurkauff, C. Cottin-Bizonne, J. Palacci, C. Ybert and L. Bocquet, Dynamic clustering in active colloidal suspensions with chemical signaling, *Phys. Rev. Lett.*, 2012, **108**, 268303.
20. T.-C. Lee, M. Alarcón-Correa, C. Miksch, K. Hahn, J. G. Gibbs and P. Fischer, Self-propelling nanomotors in the presence of strong brownian forces, *Nano Lett.*, 2014, **14**, 2407–2412.
21. M.-J. Huang, J. Schofield and R. Kapral, *Soft Matter*, 2016, **12**, 5581.
22. G. Rückner and R. Kapral, Chemically powered nanodimers, *Phys. Rev. Lett.*, 2007, **98**, 150603.
23. L. F. Valadares, Y.-G. Tao, N. S. Zacharia, V. Kitaev, F. Galembeck, R. Kapral and G. A. Ozin, Catalytic nanomotors: Self-propelled sphere dimers, *Small*, 2010, **6**, 565.
24. Y.-G. Tao and R. Kapral, Design of chemically propelled nanodimer motors, *J. Chem. Phys.*, 2008, **10**, 770.
25. L. Wang, L. Li, T. Li, G. Zhang and Q. Sun, Locomotion of chemically powered autonomous nanowire motors, *Appl. Phys. Lett.*, 2015, **107**, 063102.

26. Y.-G. Tao and R. Kapral, Self-propelled polymer nanomotors, *ChemPhysChem*, 2009, **128**, 164518.
27. M.-J. Huang and R. Kapral, Collective dynamics of diffusiophoretic motors on a filament, *Eur. Phys. J. E*, 2016, **39**, 36.
28. S. Ebbens and J. R. Howse, Direct observation of the direction of motion for spherical catalytic swimmers, *Langmuir*, 2011, **27**, 12293.
29. I. Theurkauff, C. Cottin-Bizonne, J. Palacci, C. Ybert and L. Bocquet, Dynamic clustering in active colloidal suspensions with chemical signaling, *Phys. Rev. Lett.*, 2012, **108**, 268303.
30. I. Buttinoni, J. Bialké, H. Löwen, C. Bechinger and T. Speck, Dynamical clustering and phase separation in suspensions of self-propelled colloidal particles, *Phys. Rev. Lett.*, 2013, **110**, 238301.
31. K. K. Dey, X. Zhao, B. M. Tansi, W. J. Médez-Ortiz, U. M. Córdova-Figueroa, R. Golestanian and A. Sen, Micromotors powered by enzyme catalysis, *Nano Lett.*, 2015, **15**, 8311.
32. W. Wang, W. Duan, S. Ahmed, T. E. Mallouk and A. Sen, Small power: Autonomous nano- and micromotors propelled by self-generated gradients, *Nano Today*, 2013, **8**(5), 531–554.
33. W. Wang, W. Duan, A. Sen and T. E. Mallouk, Catalytically powered dynamic assembly of rod-shaped nanomotors and passive tracer particles, *Proc. Natl. Acad. Sci. U. S. A.*, 2013, **110**, 17744.
34. W. Wang, W. Duan, S. Ahmed, A. Sen and T. E. Mallouk, From one to many: Dynamic assembly and collective behavior of self-propelled colloidal motors, *Acc. Chem. Res.*, 2015, **48**(7), 1938–1946.
35. P. Colberg and R. Kapral, Angstrom-scale chemically powered motors, *EPL*, 2014, **106**, 30004.
36. P. de Buyl and R. Kapral, Phoretic self-propulsion: a mesoscopic description of reaction dynamics that powers motion, *Nanoscale*, 2013, **5**, 1337–1344.
37. M. Yang and M. Ripoll, Simulations of thermophoretic nanoswimmers, *Phys. Rev. E*, 2011, **84**, 061401.
38. M. Yang and M. Ripoll, Thermophoretically induced flow field around a colloidal particles, *Soft Matter*, 2013, **9**, 4661–4671.
39. M. Yang, A. Wysocki and M. Ripoll, Hydrodynamic simulations of self-phoretic microswimmers, *Soft Matter*, 2014, **10**, 6208–6218.
40. A. Malevanets and R. Kapral, Mesoscopic model for solvent dynamics, *J. Chem. Phys.*, 1999, **110**, 8605.
41. A. Malevanets and R. Kapral, Solute molecular dynamics in a mesoscale solvent, *J. Chem. Phys.*, 2000, **112**, 72609.
42. R. Kapral, Multiparticle collision dynamics: Simulation of complex systems on mesoscales, *Adv. Chem. Phys.*, 2008, **140**, 89.
43. G. Gompper, T. Ihle, D. M. Kroll and R. G. Winkler, Multi-particle collision dynamics: A particle-based mesoscale simulation approach to the hydrodynamics of complex fluids, *Adv. Polym. Sci.*, 2009, **221**, 1.
44. K. Rohlf, S. Fraser and R. Kapral, Reactive multiparticle collision dynamics, *Comput. Phys. Commun.*, 2008, **179**, 132.

45. S. Y. Reigh, M.-J. Huang, J. Schofield and R. Kapral, Microscopic and continuum descriptions of janus motor fluid flow fields, *Philos. Trans. R. Soc., A*, 2016, **374**, 20160140.
46. S. Y. Reigh and R. Kapral, Catalytic dimer nanomotors: continuum theory and microscopic dynamics, *Soft Matter*, 2015, **11**, 3149–3158.
47. J. L. Anderson, M. E. Lowell and D. C. Prieve, Motion of a particle generated by chemical gradients part 1. non-electrolytes, *J. Fluid Mech.*, 1982, **117**, 107–121.
48. J. L. Anderson and D. C. Prieve, Diffusiophoresis: Migration of colloidal particles in gradients of solute concentration, *Sep. Pur. Rev.*, 1984, **13**, 67–103.
49. J. L. Anderson and D. C. Prieve, Diffusiophoresis caused by gradients of strongly adsorbing solutes, *Langmuir*, 1991, **7**, 403–406.
50. M.-J. Huang, J. Schofield and R. Kapral, Chemotactic and hydrodynamic effects on collective dynamics of self-diffusiophoretic janus motors, *New J. Phys.*, 2017, **19**, 125003.
51. T. Vicsek, A. Czirók, E. Ben-Jacob, I. Cohen and O. Shochet, Novel type of phase transition in a system of self-driven particles, *Phys. Rev. Lett.*, 1995, **75**, 1226–1229.
52. H. Chaté, F. Ginelli, G. Grégoire and F. Raynaud, Collective motion of self-propelled particles interacting without cohesion, *Phys. Rev. E*, 2008, **77**, 046113.
53. F. Peruani, A. Deutsch and M. Bär, Nonequilibrium clustering of self-propelled rods, *Phys. Rev. E*, 2006, **74**, 030904.
54. G. S. Redner, M. F. Hagan and A. Baskaran, Structure and dynamics of a phase-separating active colloidal fluid, *Phys. Rev. Lett.*, 2013, **110**, 055701.
55. M. E. Cates and J. Tailleur, When are active brownian particles and run-and-tumble particles equivalent? consequences for motility-induced phase separation, *EPL*, 2013, **101**(2), 20010.
56. J. Bialké, H. Löwen and T. Speck, Microscopic theory for the phase separation of self-propelled repulsive disks, *EPL*, 2013, **103**(3), 30008.
57. J. Palacci, S. Sacanna, A. P. Steinberg, D. J. Pine and P. M. Chaikin, Living crystals of light-activated colloidal surfers, *Science*, 2013, **339**(6122), 936–940.
58. A. Wysocki, R. G. Winkler and G. Gompper, Cooperative motion of active brownian spheres in three-dimensional dense suspensions, *EPL*, 2014, **105**(4), 48004.
59. S. C. Takatori and J. F. Brady, Towards a thermodynamics of active matter, *Phys. Rev. E*, 2015, **91**, 032117.
60. T. Speck, A. M. Menzel, J. Bialké and H. Löwen, Dynamical mean-field theory and weakly non-linear analysis for the phase separation of active brownian particles, *J. Chem. Phys.*, 2015, **142**, 224109.
61. A. Zöttl and H. Stark, Hydrodynamics determines collective motion and phase behavior of active colloids in quasi-two-dimensional confinement, *Phys. Rev. Lett.*, 2014, **112**, 118101.

62. X. Ma, K. Hahn and S. Sanchez, Catalytic mesoporous janus nanomotors for active cargo delivery, *J. Am. Chem. Soc.*, 2015, **137**, 4976.
63. S. Jiang, Q. Chen, M. Tripathy, E. Luijten, K. S. Schweizer and S. Granick, Janus particles synthesis and assembly, *Adv. Mater.*, 2010, **22**, 1060.
64. M. Ibele, T. E. Mallouk and A. Sen, Schooling behavior of light-powered autonomous micromotors in water, *Angew. Chem., Int. Ed.*, 2009, **48**(18), 3308–3312.
65. S. Thakur and R. Kapral, Collective dynamics of self-propelled sphere-dimer motors, *Phys. Rev. E*, 2012, **85**, 026121.
66. P. H. Colberg, S. Y. Reigh, B. Robertson and R. Kapral, Chemistry in motion: tiny synthetic motors, *Acc. Chem. Res.*, 2014, **47**, 3504.
67. O. Pohl and H. Stark, Dynamic clustering and chemotactic collapse of self-phoretic active particles, *Phys. Rev. Lett.*, 2014, **112**, 238303.
68. S. Saha, R. Golestanian and S. Ramaswamy, Clusters, asters, and collective oscillations in chemotactic colloids, *Phys. Rev. E*, 2014, **89**, 062316.
69. O. Pohl and H. Stark, Self-phoretic active particles interacting by diffusiophoresis: A numerical study of the collapsed state and dynamic clustering, *Eur. Phys. J. E*, 2015, **38**, 93.
70. P. Colberg and R. Kapral, Many-body dynamics of chemically-propelled nanomotors, *J. Chem. Phys.*, 2017, **147**, 064910.
71. Y. Fily and M. C. Marchetti, Athermal phase separation of self-propelled particles with no alignment, *Phys. Rev. Lett.*, 2012, **108**, 235702.
72. Y. Fily, S. Henkes and M. C. Marchetti, Freezing and phase separation of self-propelled disks, *Soft Matter*, 2014, **10**, 2132.
73. T. Speck, J. Bialké, A. M. Menzel and H. Löwen, Effective cahn-hilliard equation for the phase separation of active brownian particles, *Phys. Rev. Lett.*, 2014, **112**, 218304.
74. J. Stenhammar, D. Marenduzzo, R. J. Allen and M. E. Cates, Phase behaviour of active brownian particles: the role of dimensionality, *Soft Matter*, 2014, **10**, 1489.
75. J. K. G. Dhont, *An Introduction to Dynamics of Colloids*, Elsevier, Amsterdam, 1996.
76. J. Happel and H. Brenner, *Low Reynolds Number Hydrodynamics: with Special Applications to Particulate Media*, Springer, Netherlands, 2012.
77. S. Kim and S. J. Karrila, *Microhydrodynamics: Principles and Selected Applications*, Butterworth-Heinemann, Boston, MA, 2013.
78. A. Baskaran and M. C. Marchetti, Statistical mechanics and hydrodynamics of bacterial suspensions, *Proc. Natl. Acad. Sci. U. S. A.*, 2009, **106**, 15567.
79. D. Saintillan and M. J. Shelley, Emergence of coherent structures and large-scale flows in motile suspensions, *J. R.. Soc., Interface*, 2012, **9**(68), 571–585.
80. S. E. Spagnolie and E. Lauga, Hydrodynamics of self-propulsion near a boundary: predictions and acuracy of far-field approximations, *J. Fluid Mech.*, 2016, **700**, 105.

81. M. C. Marchetti, J. F. Joanny, S. Ramaswamy, T. T. Liverpool, J. Prost, M. Rao and R. A. Simha, Hydrodynamics of soft active matter, *Rev. Mod. Phys.*, 2013, **85**, 1143.
82. A. Bricard, J.-B. Caussin, N. Desreumaux, O. Dauchot and D. Bartolo, Emergence of macroscopic directed motion in populations of motile colloids, *Nature*, 2013, **503**, 95.
83. J. Blaschke, M. Maurer, K. Memon, A. Zöttl and H. Stark, Phase separation and coexistence of hydrodynamically interacting microswimmers, *Soft Matter*, 2016, **12**, 9821.
84. S. Saha, R. Golestanian and S. Ramaswamy, Clusters, asters, and collective oscillations in chemotactic colloids, *Phys. Rev. E*, 2014, **89**, 062316.
85. O. Pohl and H. Stark, Self-phoretic active particles interacting by diffusiophoresis: A numerical study of the collapsed state and dynamic clustering, *Eur. Phys. J. E*, 2015, **38**(8), 93.
86. M. Wagner and M. Ripoll, Hydrodynamic front-like swarming of phoretically active dimeric colloids, *Europhys. Lett.*, 2017, **119**, 66007.
87. M.-J. Huang, J. Schofield and R. Kapral, Transport in active systems crowded by obstacles, *J. Phys. A: Math. Theor.*, 2017, **50**, 074001.